Map with more than 100 coexisting low-period periodic attractors

Ulrike Feudel,[1,2] Celso Grebogi,[1,3,4] Brian R. Hunt,[4] and James A. Yorke[3,4]
[1]*Laboratory for Plasma Research, University of Maryland, College Park, Maryland 20742*
[2]*Max-Planck-Arbeitsgruppe Nichtlineare Dynamik, Universität Potsdam, PF 601553, D-14415 Potsdam, Germany*
[3]*Department of Mathematics, University of Maryland, College Park, Maryland 20742*
[4]*Institute for Physical Science and Technology, University of Maryland, College Park, Maryland 20742*
(Received 26 October 1995)

We study the qualitative behavior of a single mechanical rotor with a small amount of damping. This system may possess an arbitrarily large number of coexisting periodic attractors if the damping is small enough. The large number of stable orbits yields a complex structure of closely interwoven basins of attraction, whose boundaries fill almost the whole state space. Most of the attractors observed have low periods, because high period stable orbits generally have basins too small to be detected. We expect the complexity described here to be even more pronounced for higher-dimensional systems, like the double rotor, for which we find more than 1000 coexisting low-period periodic attractors.
[S1063-651X(96)04506-0]

PACS number(s): 05.45.+b

I. INTRODUCTION

Nonlinear dynamical systems often exhibit many rich and varied behaviors of which stationary, periodic, quasiperiodic, and chaotic attractors are some of the typical long-term behaviors. A general approach in studying the *complexity* of such systems involves investigating their dynamics as some system parameters are varied. This method yields an analysis of qualitative changes, known as bifurcations, resulting in a change of the number of attractors, their type (periodic, quasiperiodic, chaotic) and/or their stability. Thus far, a large body of work has concentrated on low-dimensional systems where only one or two attractors dominate the system's behavior. However, it is expected that many systems in nature, in particular coupled systems, are more appropriately modeled by dynamical systems that have multiple coexisting attractors. The behavior of such systems will be more complex since there is the added feature of interactions among the various attractors and their basins [1–4]. The purpose of this paper is to study the complexity of such systems using a prototype model which exhibits an arbitrarily large number of coexisting attractors, depending on a parameter. The phenomenon described here is different from the Newhouse phenomenon in which infinitely many attractors can coexist [5,6], but only for special parameter values [7,8].

The model for a periodically kicked mechanical rotor yields a two-dimensional map which can be used as such a prototype. The rotor map depends on two parameters, forcing (kick amplitude) and damping. In the limit of maximal damping, the system reduces to a one-dimensional circle map with a zero rotation number exhibiting the Feigenbaum scenario to chaos. Without damping we obtain the area-preserving standard map introduced by Chirikov [9] and widely studied by many authors [10]. This map, which we refer to as the Hamiltonian case of the rotor map, is believed to possess infinitely many (center) stable periodic orbits, each of which turns into a sink when a small amount of dissipation is applied. For given values of the dissipation and forcing, we expect that only finitely many sinks coexist. The other sinks are shifted to higher parameter values. Nonetheless it is easy to obtain system parameters for which the number of attractors is very high. The aim of this paper is to study the appearance and disappearance of these mostly low-period periodic attractors and their basins of attraction.

The paper is organized as follows. Section II is devoted to the model system and its behavior in the Hamiltonian case as well as the small dissipation case. A study of the system's behavior in state space for a fixed set of the forcing and damping parameters is presented. We discuss the number of attractors and their basins depending on the period. The box dimension of the basin boundaries is estimated. The entire bifurcation structure is considered in Sec. III; the lifetime of the stable periodic orbits of different periods in parameter space depending on forcing and damping is studied. Section IV gives a summary of the results.

II. THE SINGLE ROTOR, THE NUMBER OF ATTRACTORS AND THEIR BASINS

A suitable model for the study of systems with a large number of coexisting attractors is the kicked single rotor, which describes the time evolution of a mechanical pendulum kicked at times nT, $n=1,2,\ldots$, with a constant force f_0. From the original differential equation for the phase of the pendulum one can derive a map [11] which is related to the state of the system just after successive kicks

$$x_{k+1}=x_k+y_k(\mathrm{mod}\,2\pi),$$

$$y_{k+1}=(1-\nu)y_k+f_0\sin(x_k+y_k), \tag{1}$$

where x corresponds to the phase and y to the angular velocity. The damping parameter ν is connected to the energy dissipation and varies between 0 (Hamiltonian system without damping) and 1 (very strong damping). For these two limiting cases the behavior of the system is well known [12–14].

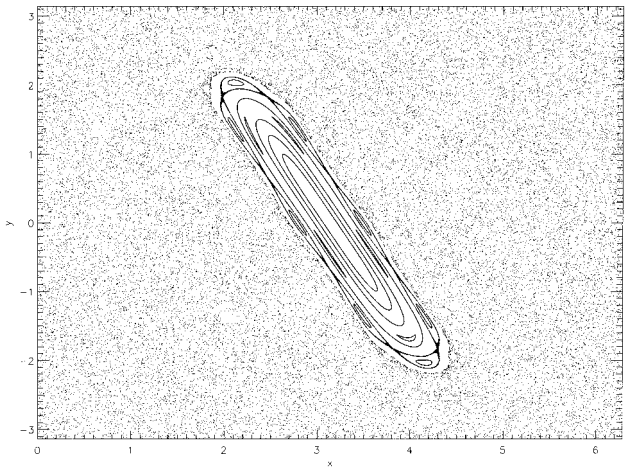

FIG. 1. Phase portrait for the single rotor with no damping ($\nu=0$) at $f_0=4.0$. This is the period doubling point for the main fixed point ($x=\pi$, $y=0$). Around this major periodic island we find chaotic behavior, all KAM invariant circles are destroyed. There are identical islands at ($x=\pi$, $y=m2\pi$) for all integers m but all coincide on the torus.

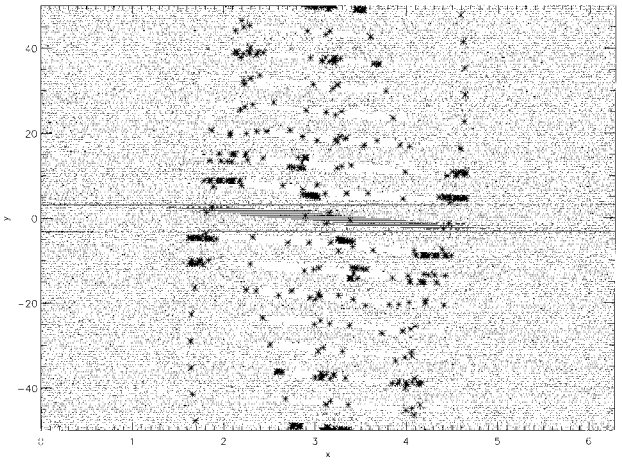

FIG. 2. The stars show the location of the attracting periodic orbits of the single rotor for the same forcing as in Fig. 1 ($f_0=4.0$) but with small damping ($\nu=0.02$). All attractors have been obtained by iterating 10^6 initial conditions on a grid in the region $[0,2\pi]\times[-200,200]$. To make the results visible, this picture shows only the region with $|y|<50$. Some of the fixed point attractors have already undergone period doubling, some of them not. The black dots indicate which initial points on the same grid have trajectories that are attracted to the orbit with the largest basin of attraction.

For very strong damping we observe the usual Feigenbaum scenario for the transition to chaos, whereas for the Hamiltonian case the state space consists of a chaotic sea interspersed with periodic islands. In between these two limiting cases the system's behavior is not so well understood. The crossover, however, between the universal constants for the period doubling cascade has been studied [15,16] as well as the transition between Hamiltonian and dissipative chaos [17,18].

In particular, close to the Hamiltonian case, i.e., with a small amount of damping, the system exhibits a rich dynamical behavior which is mainly dominated by the appearance and disappearance of periodic attractors of different periods leading to a very complex bifurcation diagram. The complexity of the bifurcation structure varies strongly depending on the strength of the forcing f_0 and the damping ν. Actually, the number of attractors can, in principle, be arbitrarily high by choosing the damping small.

A. No dissipation

Because we are interested in the system's behavior close to the Hamiltonian case, let us briefly recall some properties of (1) for zero damping ($\nu=0$). There exists regular motion around the stable periodic orbits of the map (1) as well as Kolmogorov-Arnold-Moser (KAM) invariant circles. On the other hand there also exist regions with persistent chaotic motion. Both regions are complexely interwoven depending on the nonlinearity parameter f_0. Furthermore, the Lebesgue measures of these regular and chaotic regions vary with the system parameters.

In the Hamiltonian case, the second equation in (1) for the angular velocity y can be taken modulo 2π too, and the dynamics are then located on the torus $[0,2\pi]\times[0,2\pi]$. Therefore, periodic orbits, which are solutions of Eqs. (1), resides on the torus. As such, each of the periodic orbits, as seen in Fig. 1, represents a whole family of overlapping periodic orbits in which the velocities y differ by multiples of 2π, e.g., the family of period 1 orbits has the coordinates ($x^*=\pi$, $y^*=m2\pi$) with $m=0,\pm1,\ldots$ and, because of the modulo 2π, they are all in the same location on the torus. We distinguish between two types of periodic orbits. The primary families (or islands) are the fixed points (period 1) and the higher period periodic orbits (period >1) that exist for zero nonlinearity f_0. They make up the largest regions of regular motion in the state space and are surrounded by small islands of stability. These small islands have higher period and are the secondary families that exist only for a nonzero nonlinearity. The secondary orbits have in general much smaller stability regions than the primary ones.

B. Small dissipation

The structure shown in Fig. 1 does not persist if a small amount of dissipation is introduced. The periodic orbits become sinks and the chaotic motion is replaced by long chaotic transients that occur before the trajectory eventually settles down in one of the sinks [18]. Furthermore, the state space is no longer a torus; the motion takes place on the cylinder $[0,2\pi]\times R$. The dissipation leads to a separation of the overlapping periodic orbits belonging to a given family with increasing modulus of the velocities on the cylinder. For example, the fixed points of the period 1 family, which are represented by one point in Fig. 1, are now distinguished by different phase values and different velocity values that differ by $\pm m2\pi$ with m an integer. Figure 2 is a picture in state space showing attractors with higher and higher velocities that are surrounded by sinks arising from former secondary islands. Figure 3 shows a blowup of the indicated region around $y=0$ in Fig. 2. Black points are attracted to the attractor that was the primary island while white points are attracted to other attractors.

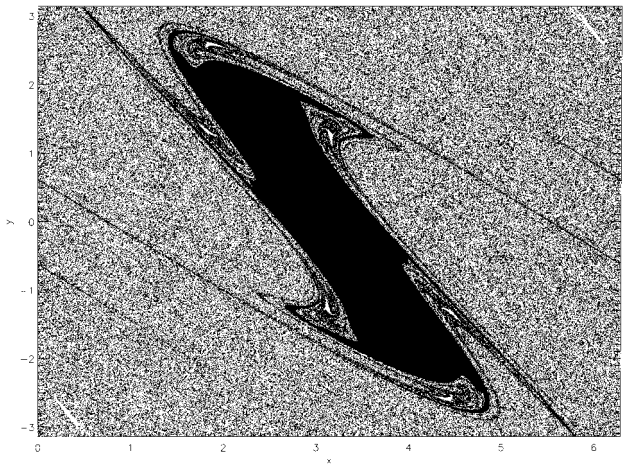

FIG. 3. The largest basin of attraction in the system (365 004 points). This is an enlargement of the region indicated by the rectangle in Fig. 2. We have iterated 10^6 initial conditions on a grid in the region shown $[0,2\pi]\times[-\pi,\pi]$. The main orbit has already undergone period doubling at this parameter value.

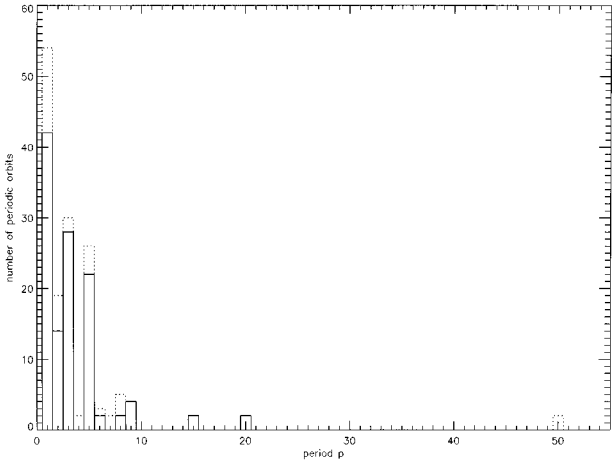

FIG. 4. Number of periodic attractors for the damped single rotor vs their period for $\nu=0.02$ and $f_0=4.0$. The solid columns show the results using 10^4 initial conditions while the dashed columns is for 10^6 initial conditions.

In contrast to the undamped case where the number of stable periodic orbits is infinite, we believe that there are a finite number of attractors in the damped case, though this number can be very large. In particular, when the damping is positive there is a bounded cylinder which contains all of the attractors. From the second equation in map (1) we see that

$$|y_{k+1}|\leqslant(1-\nu)|y_k|+f_0. \tag{2}$$

Thus if $|y_k|>f_0/\nu$ then $|y_{k+1}|<|y_k|$. It follows that all trajectories are eventually trapped in the region $[0,2\pi]\times[-y_{\max},y_{\max}]$, where

$$y_{\max}=\frac{f_0}{\nu}. \tag{3}$$

Therefore $y_{\max}$ provides a limit for the modulus of the velocities for attractors arising from former primary and secondary islands as well.

To estimate the number of coexisting periodic orbits, we iterate 10^4 initial conditions on a grid of 100×100 in the rectangle $[0,2\pi]\times[-y_{\max},y_{\max}]$. The accuracy with which each periodic orbit P_N of period N is given by $\|\mathbf{x}(N)-\mathbf{x}(0)\|\leqslant10^{-8}$. Our procedure for finding periodic orbits is then the following. First, we fix all parameters, say, the damping at $\nu=0.02$ and the forcing at $f_0=4.0$. For this particular parameter set we find 118 different periodic attractors in the rectangle $[0,2\pi]\times[-200,200]$. In this case, we find no initial conditions that do not converge to periodic attractors. In Fig. 4, we show a histogram with the number of periodic attractors of each period. It turns out that most of the periodic attractors have low periods (<10); stable higher period orbits are found rarely. It is worth mentioning that the number of attractors obtained depends on the resolution of the initial conditions in the state space. If we increase the number of initial conditions to 10^5 and even 10^6 points the total number of periodic attractors found rises to 146 and 153, respectively. A finer resolution in state space yields also more stable orbits with rather high periods. For 10^4 initial conditions the highest period found is 20, whereas with 10^6 initial conditions we were able to detect a period 50 attractor. As discussed below, higher period periodic orbits typically have a smaller basin of attraction and, therefore, need a finer resolution grid to find them.

Let us now look at the size of the basins of the periodic attractors. Figure 2 shows, besides the attractors, the basin (black dots) of the main orbit of the P_1 family. This orbit, which we denote by P_1^0, has zero velocity and a phase $x=\pi$. It marks the location of the symmetry axis for the system. The other P_1 orbits have coordinates $P_1^m=(x=x^*,\ y=m2\pi)$ with $m=\pm1,\pm2,\ldots$. Velocities of a different sign correspond to clockwise and counterclockwise rotation. Their basins, as well as the basins of other P_N orbits for $N>1$, appear as white dots in Fig. 2. The P_1^0 basin is the largest one for the system and, in general, all basins of the P_1 orbits are relatively large compared to the others. They make up about 84.4% of the whole number of initial conditions in the space of initial conditions under consideration and only the remaining 15.6% of all initial points belong to the basins of the higher period periodic orbits. The basins of attractors with periods >10 cover only 0.0067% of the space of initial conditions. For the size of the basins within the P_1 family we obtain a rather quick decrease in the basin size with increasing values of the velocity for the initial conditions being considered, as shown in Fig. 5. (The oscillations in the size of the basins of the primary P_1 attractors is related to the existence of secondary sinks surrounding the primary ones. They ''eat up'' a part of the basins of the primary orbits they are connected with.) Hence periodic attractors of the same family but with higher velocities are more difficult to find because of their small basins. For higher period periodic attractors the situation is even worse because even the largest basins of a given family occupy only a small part of the considered state space (9.1% for all P_5 orbits and 4.97% for all P_3 orbits). Therefore increasing the number of initial conditions leads to a higher number of attractors since stable orbits with even smaller basins become ''visible.''

If we consider for fixed parameters (e.g., $f_0=4.0$) the

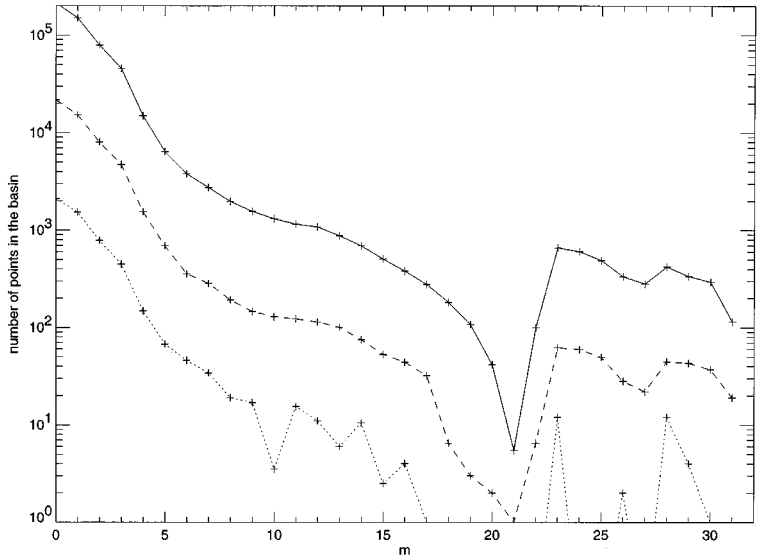

FIG. 5. The attractors of the P_1 family have y values that are $m2\pi$ for an integer m. The solid line shows the number of initial points, from a grid of 10^6 initial conditions, that are in the basin of the mth attractor in P_1 for $m \geqslant 0$. The results for the symmetric $-m$ basin are the same as the $+m$ basin. The dashed line is for 10^5 initial conditions while the dotted line is for 10^4 initial conditions.

number of attractors found in each family as a function of the number of initial conditions, we observe for small numbers of initial conditions ($<2\times10^4$) a rather rapid increase in the number of attractors followed by a saturation for a higher number of initial conditions. The starting point of the saturation is different for different periods; for higher periods one needs more initial conditions to achieve a saturation. For the low-period periodic attractors (period <10), which are the main contribution to the total number of attractors, this saturation starts for initial conditions $>5\times10^4$, while the total number of attractors has not yet saturated for 10^5 initial conditions.

The percentages of initial state space occupied by the basins of the different families of attractors remains approximately the same as the number of initial conditions is varied. We find that at least 60% (when we take 10^6 initial conditions) of the attractors under consideration have basins smaller than 0.1% in state space.

For the remaining computations in this paper we use 10 000 initial conditions. As a result, the periodic orbits under consideration are those whose basins are larger than $\frac{1}{10\,000}$ of the state space.

Another interesting observation is that the basins seem to have fractal boundaries which appear to spread over most of the state space (see Fig. 3). This yields a complex interwoven structure of the basins. To illustrate this complicated network of basins we present a small basin of a secondary sink (P_3) in Fig. 6 showing points spread over most of the state space. Extremely small changes in the initial conditions are sufficient to shift a point from one basin to another. This high sensitivity to the final state can be measured by computing the uncertainty exponent, which is related to the dimension of the boundary [19].

Suppose we take 10 000 randomly chosen initial conditions $[x(0),y(0)]$ and determine for each of them the attractor they converge to. Now we change the initial conditions slightly to $[x(0)+\epsilon,y(0)]$ and measure the fraction of initial conditions $f(\epsilon)$ that change from one basin to another. This fraction of initial conditions is said to be uncertain with respect to this perturbation of size ϵ. It has been argued in [20] and proved in [21] for Axiom A systems that this fraction $f(\epsilon)$ generally scales with ϵ as

$$f(\epsilon)\sim\epsilon^{\alpha}, \tag{4}$$

where α is the ''uncertainty exponent.'' This exponent is typically related to the box counting dimension d of the basin boundary by $\alpha=D-d$, where D is the dimension of the state space. The uncertainty exponent is estimated from the slope in the log $f(\epsilon)$–logϵ plot as shown in Fig. 7. For damping $\nu=0.05$ we get $\alpha=0.006\,41$ and, hence, $d=1.993\,59$; for $\nu=0.02$ we obtain $\alpha=0.001$ and $d=1.999$, i.e., the basin boundary is nearly two dimensional. Furthermore, it is interesting to note that for $\epsilon=10^{-10}$ about 90% of the initial points changed to another basin. This large percentage can be regarded as an additional indication of the high complexity of the basin structure. Let us ask now which accuracy would be necessary to predict the final state with a probability of 99%, i.e., the fraction of uncertain initial conditions shall be 0.01. As a result we obtain an accuracy

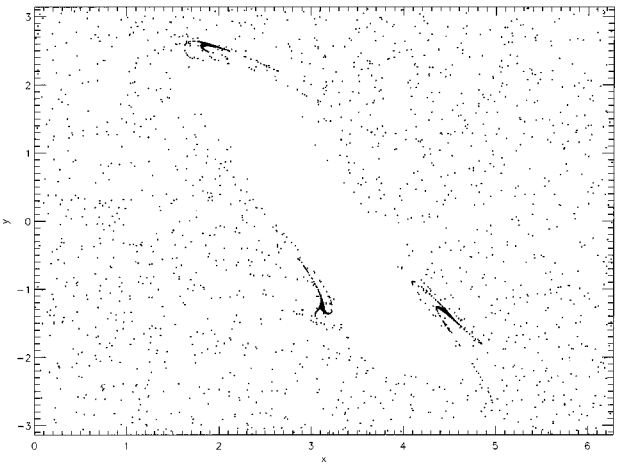

FIG. 6. Basin of attraction of one orbit of the period 3 family P_3 in the same part of the state space as Fig. 3. This basin is made up of 2427 points out of 10^6 initial conditions in $[0,2\pi]\times[-\pi,\pi]$.

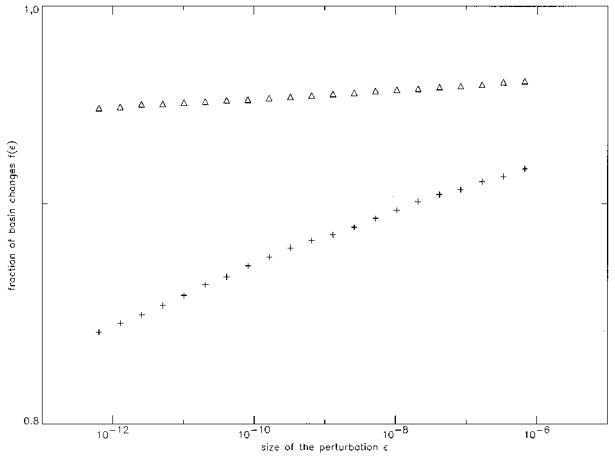

FIG. 7. Fraction of uncertain initial conditions $f(\epsilon)$ vs size of the perturbation ϵ for forcing $f_0=4.0$ and two different values of the damping: $\nu=0.05$ (+) and $\nu=0.02$ (Δ). We iterate a sufficient number of initial conditions such that the number of initial conditions that change basins with a perturbation of size ϵ is 10 000.

$$\epsilon \approx f(\epsilon)^{1/\alpha} = 0.01^{1/0.001} = 10^{-2\,000}, \tag{5}$$

which is not realizable with standard floating-point numerical calculations.

III. MULTIPLE COEXISTING ATTRACTORS

So far we have only discussed the number of attracting periodic orbits for a fixed forcing and damping. Now we vary the forcing in order to get the number of coexisting attractors in an interval, say, $f_0 \in [0,5]$. The damping is still kept fixed at $\nu=0.02$. To obtain a good estimate for the number of attractors we have to adjust the cylinder of initial conditions $[0,2\pi]\times[-y_{\max},y_{\max}]$ when changing f_0 according to (3). Figure 8 presents the extremely complex bifurcation structure obtained for this parameter set. Nevertheless, the number of attractors shown in Fig. 9, though being more than 100 for some f_0, is only an approximation since some of the attractors have very small basins of attraction as discussed above. Therefore we cannot find them with only 10^4 or 10^5 initial conditions in a large cylinder.

Let us discuss the general properties of the bifurcation diagram and the corresponding number of attractors [Figs. 8(a), 8(b), 9]. As already mentioned, the map (1) possesses a symmetry with respect to the orientation of the rotation of the rotor. Therefore the dynamics are symmetric with respect to $y=0$ and $x=\pi$ corresponding to clockwise and counterclockwise motion. That means that to each periodic orbit $P_N(x_k^*,y_k^*)$, $k=1,\ldots,N$, we find another orbit with $(2\pi-x_k^*,-y_k^*)$. Most of the periodic attractors appear as a result of a saddle-node bifurcation. With a further increase of the forcing f_0 they undergo a period doubling cascade into chaos. If P_N is invariant with respect to the symmetry transformation then a symmetry breaking bifurcation in form of a pitchfork occurs before the period doubling cascade [22]. The intervals of chaotic behavior are very tiny and therefore, not visible in the present resolution in parameter space. For the whole parameter interval we find only less than 1% of initial conditions which do not converge to a periodic orbit after 25 000 iterates. But for these not converging orbits we did not check for chaos by calculating Lyapunov exponents.

Looking at the number of periodic attractors (Fig. 9) we observe that the number of periodic attractors fluctuates under the variation of f_0. These fluctuations reflect the fact that a large number of the total number of periodic attractors exist only on a very small interval along the f_0 axis which has a resolution of $\delta f_0=0.001$. In the bifurcation diagram these attractors are denoted only by a few points and they would be seen as periodic orbits possessing a period doubling cascade in a higher resolution plot. As discussed in the preceding section, the number of counted attractors depends strongly on the number of initial conditions used. With a larger number of initial conditions more attractors with smaller basins are detected. Since the number of attractors for the low-period periodic orbits has already saturated for 10^5 initial conditions, the solid line in Fig. 9 can be regarded as a good approximation of the total number of attractors.

The stability region of a particular periodic orbit can be regarded as the interval between its appearance and disappearance. Multistability refers to the overlapping of these intervals belonging to different periodic orbits in parameter space. To study this stability region of periodic orbits in parameter space we consider the distance between the saddle-node bifurcation f_0^{sn} and the first period doubling f_0^{pd} as a measure for their extension in parameter space. We call this distance $\Delta f_0=f_0^{\mathrm{pd}}-f_0^{\mathrm{sn}}$ the lifetime of the stable periodic orbit in parameter space. The length of this parameter interval Δf_0 is different for each periodic orbit, and varies strongly with damping ν. To get a better insight into the global behavior we investigate these stability regions $[f_0^{\mathrm{pd}},f_0^{\mathrm{sn}}]$ of P_N in the $f_0-\nu$ space.

For the period 1 family P_1^m this interval can be computed analytically. First one has to compute the period 1 fixed points, that result from the equations $x_{k+1}-x_k=0$ and $y_{k+1}-y_k=0$. The solution of

$$y^*=0 \pmod{2\pi},$$

$$-\nu y^*+f_0\sin(x^*+y^*)=0 \tag{6}$$

yields the stable fixed points $(x^*=\pi,y^*=0)$ and $[\sin(x^*+m2\pi)=\nu m2\pi/f_0,y^*=m2\pi]$ with $m=\pm1,\pm2,\ldots$. The saddle-node bifurcation occurs when the corresponding Jacobian matrix $\mathbf{J}|_{x=x^*,y=y^*}$ has an eigenvalue $\lambda_{\mathrm{sn}}=+1$, whereas the period doubling corresponds to an eigenvalue $\lambda_{\mathrm{pd}}=-1$ of the same matrix. Solving the equation $|\mathbf{J}-\lambda\mathbf{I}|=0$ for $\lambda_{\mathrm{sn}}=+1$ and $\lambda_{\mathrm{pd}}=-1$ for each pair (x^*,y^*) yields the curves f_0^{sn} and f_0^{pd} in the parameter space where the eigenvalue condition for each of these two bifurcations is fulfilled. Because of their different symmetry properties, we consider the fixed points $P_1^0=(\pi,0)$ and $P_1^m=(x^*,m2\pi)$, $m=\pm1,\pm2,\ldots$ separately. The fixed point $(\pi,0)$ appears for all ν at $f_0=0$. This attractor undergoes a period doubling bifurcation at $f_0=4-2\nu$. The attractor with double period is invariant under the symmetry transformation; therefore, a pitchfork bifurcation at $f_0=(2-\nu)\pi$ occurs before the period doubling cascade starts [13]. The lifetime of the P_1^0 orbit varies linearly with the damping as $\Delta f_0=4-2\nu$. For the other P_1^m fixed points

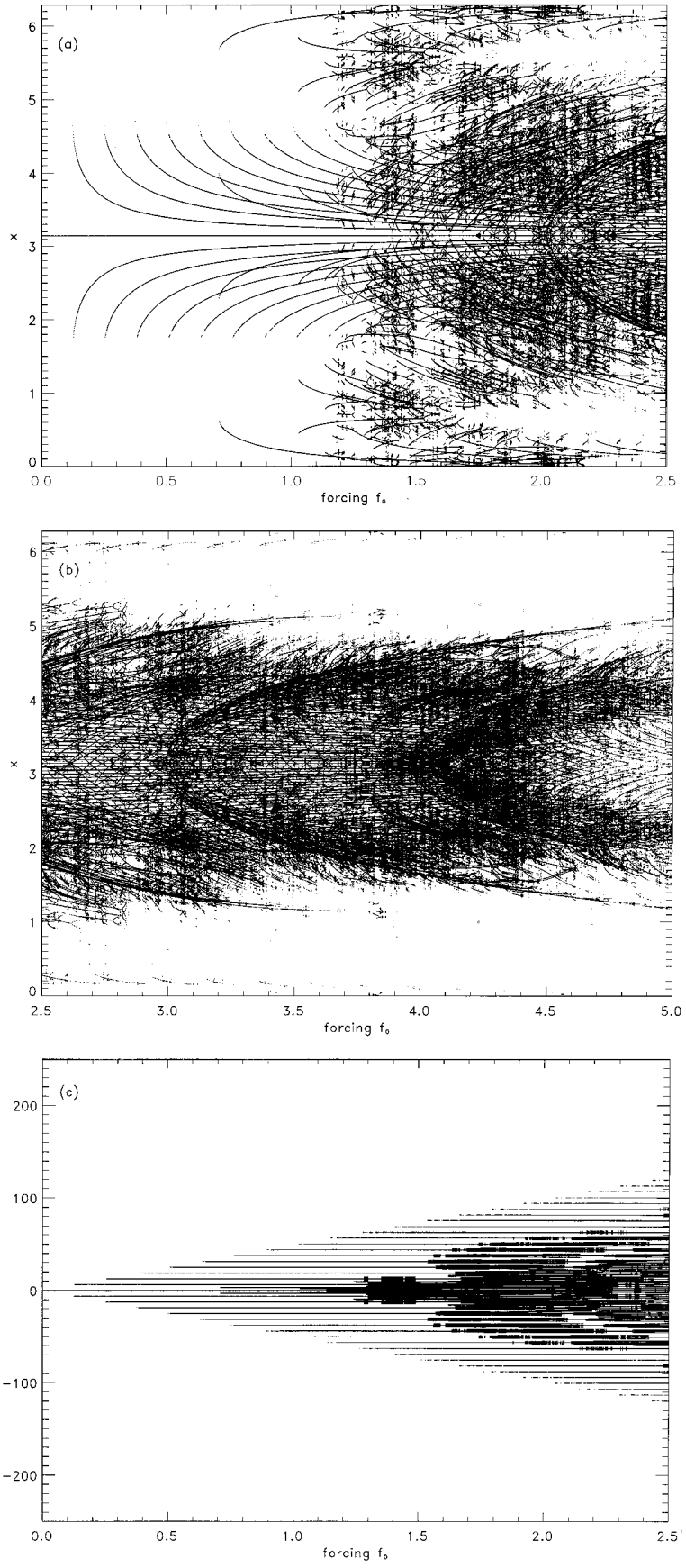

FIG. 8. Periodic attractors for fixed damping ($\nu=0.02$) depending on the forcing f_0 in the interval $[0,5]$: (a) phase of the rotor x, $f_0 \in [0,2.5]$; (b) phase of the rotor x, $f_0 \in [2.5,5]$; (c) angular velocity of the rotor y, $f_0 \in [0,2.5]$; (d) angular velocity of the rotor y, $f_0 \in [2.5,5]$. The number of initial conditions used is 10^4.

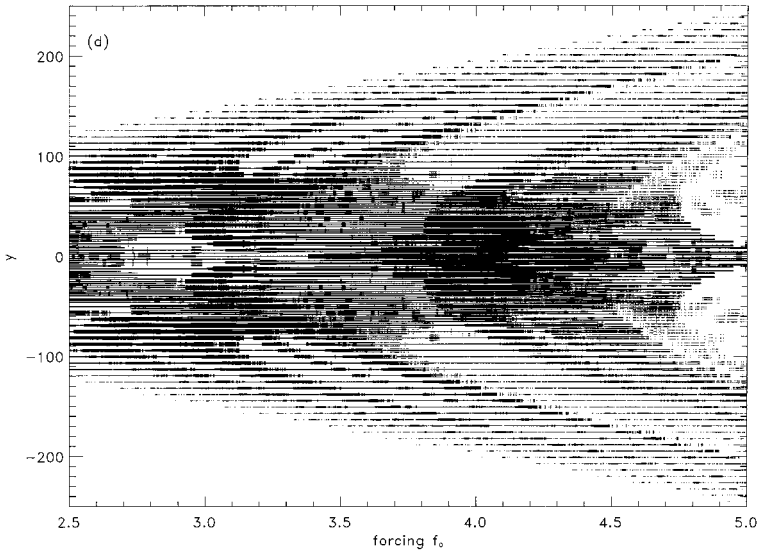

FIG. 8 (*Continued*).

the behavior is different. However it is the same for each pair of orbits with the same $|m|$. Their saddle node bifurcation occurs at

$$f_0^{\mathrm{sn}} = \nu |m| 2\pi \tag{7}$$

whereas the first period doubling occurs at

$$f_0^{\mathrm{pd}} = \sqrt{(\nu m 2\pi)^2 + 4(2-\nu)^2}. \tag{8}$$

The lifetime of these fixed points is thus

$$\Delta f_0 = f_0^{\mathrm{pd}} - f_0^{\mathrm{sn}} = \sqrt{(\nu m 2\pi)^2 + 4(2-\nu)^2} - \nu |m| 2\pi. \tag{9}$$

Both orbits with the same $|m|$ have the same stability interval. The stability intervals of the first six orbits of the P_1 family ($m = \pm 1, \pm 2, \pm 3$) are shown in Fig. 10(a). For the other orbits $P_N^m (N \neq 1)$ these intervals Δf_0 can be obtained numerically using continuation methods [23]. Figure 10(b) shows the results for six orbits of the secondary P_3 family. From these computations we can distinguish the families of periodic orbits according to the classification in the undamped case mentioned above. Each of these families is characterized by a special form of these lifetime intervals in the $f_0 - \nu$ space. The saddle-node bifurcations, i.e., the appearance of orbits of primary families, can be continued to $f_0 = 0$ at $\nu = 0$, whereas secondary families always need a finite forcing $f_0 \neq 0$ to be excited at $\nu = 0$. All bifurcation points of different orbits of the same family converge to the same bifurcation points in the Hamiltonian case.

As was already pointed out in [13], all of the saddle-node bifurcations and period doublings can be continued to the limit of very strong damping $\nu = 1$. That means that all periodic orbits present in the Hamiltonian case can be found in the dissipative case too. But the forcing needed to excite these orbits increases with increasing velocity. For strong damping it turns out that the stability intervals do not overlap any more, so that orbits of the same family do not coexist. This results in fewer and fewer coexisting orbits with increasing damping and, hence, a decrease in the total number of orbits for a given forcing interval. Besides the shift to higher forcing we also notice that the lifetime of all orbits gets smaller with increasing damping [Figs. 10(a), 10(b)].

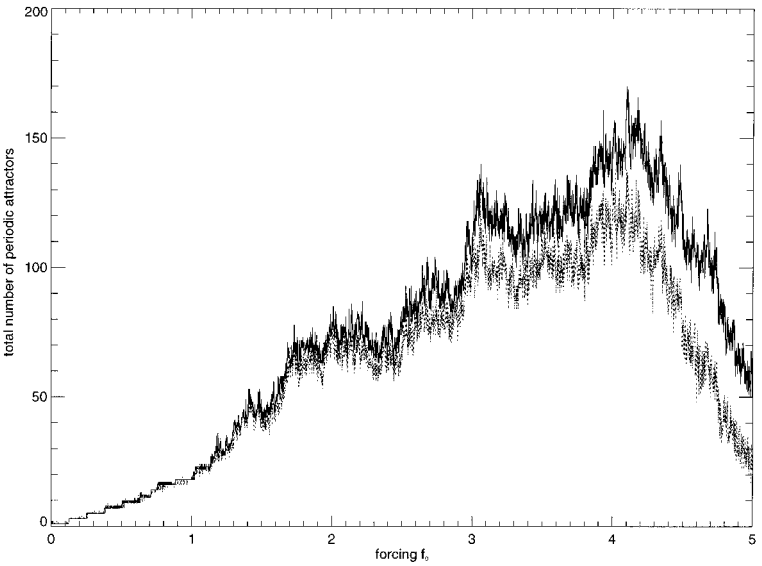

FIG. 9. Total number of periodic attractors depending on the forcing f_0: The dashed line shows the number of periodic attractors shown in Fig. 8 using 10^4 initial conditions. For the solid line we used 10^5 initial conditions.

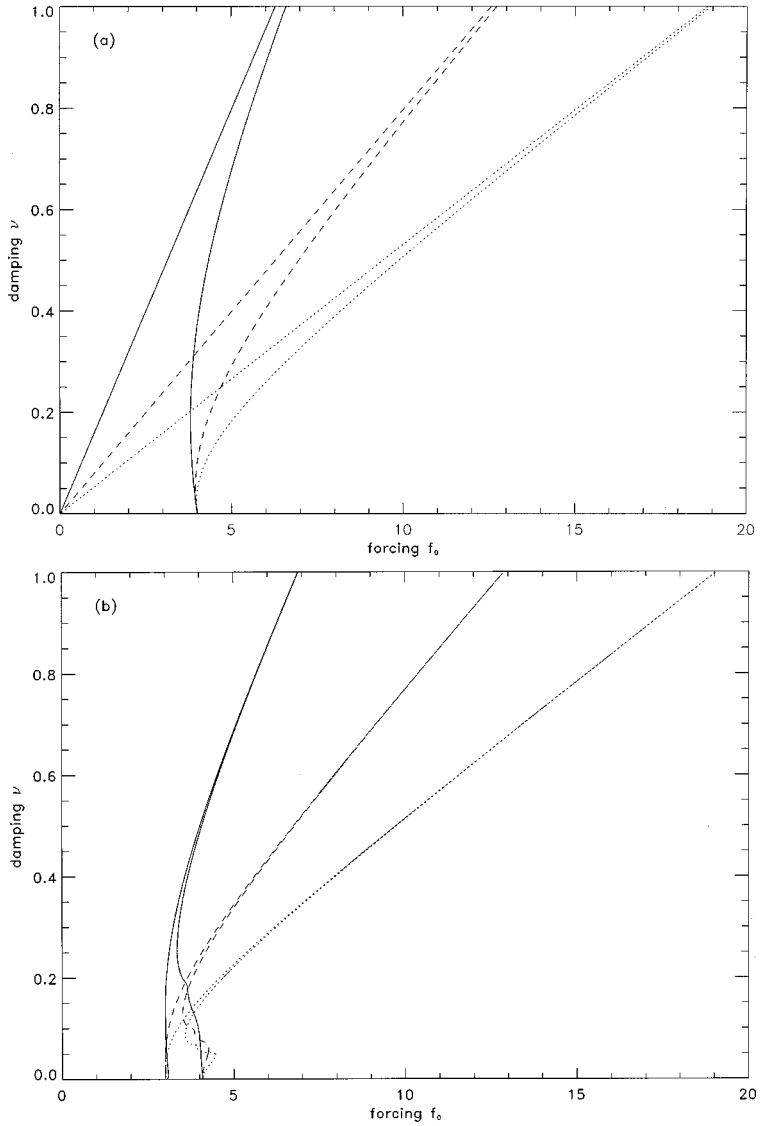

FIG. 10. (a) The lifetime intervals of the first orbits of the primary family P_1: with $m=\pm 1$ (solid lines), $m=\pm 2$ (dashed lines), and $m=\pm 3$ (dotted lines) in the forcing-damping parameter space. These intervals of stability for each orbit extend between the saddle-node bifurcation (left curve) and the first period doubling (right curve); (b) the lifetime intervals of the first orbits of the secondary family P_3: $m=\pm 1$ (solid lines), $m=\pm 2$ (dashed lines), and $m=\pm 3$ (dotted lines).

This means that even if the forcing is sufficient to obtain a specific periodic orbit we may not observe it if its lifetime in parameter space is smaller than the resolution δf_0 used. This argument holds especially for higher period periodic orbits [compare the lifetime intervals for the P_1 and P_3 families in Figs. 10(a), 10(b)]. These two mechanisms — *the shift to higher forcing and the shrinking of lifetime intervals* — are the main reasons that the number of orbits in a specific forcing interval decreases rapidly with increasing damping. For illustration we present another bifurcation diagram (Fig. 11) where the damping is still small ($\nu=0.05$) but larger than in Fig. 8. Since we restrict our consideration to the interval $f_0 \in [0,5]$ fewer orbits are found; in particular the number of high period periodic attractors decreases much faster than the number of the low period ones.

Let us now discuss the opposite case, how the number of attractors rises as we come close to the Hamiltonian case. The two mechanisms mentioned above can be reformulated to explain the rapid increase in the number of attractors as damping approaches zero, i.e., $\nu=0$. First, the shift in the appearance of periodic orbits towards lower forcing values yields an increased overlapping of the stability intervals of orbits of the same family. Second, the lifetimes of stable orbits in parameter space get larger with decreasing damping. For the P_1^m orbits we get an analytical expression for the number N_{p1} of stable orbits for fixed f_0. According to (7) two P_1 attractors with velocities $y^*=\pm m2\pi$ arise if $f_0^{\mathrm{sn}}=\nu|m|2\pi$. Now, we fix f_0 and vary the damping ν. With decreasing damping, beginning from 1, we always cross a saddle-node bifurcation curve if $f_0=\nu|m|2\pi$ or in other words, if $f_0/2\pi\nu$ gives the next integer value m. Each crossing gives us 2 additional P_1 attractors. Therefore the number N_{p1} can be computed as follows:

$$N_{p1}=2\mathcal{I}\left(\frac{f_0}{2\pi\nu}\right)+1, \tag{10}$$

where $\mathcal{I}$ denotes the integer part of the expression in brackets. The additional $+1$ refers to the solution $(x^*=\pi,\ y^*=0)$. The validity of (10) is restricted to that f_0 interval where none of the P_1^m orbits has undergone a period doubling. The number of P_1 orbits increases rapidly when the damping goes to zero. We expect that the same scaling $N_{pN}\sim 1/\nu$ holds for higher periods as well. Thus adding a small amount of damping we expect a finite number

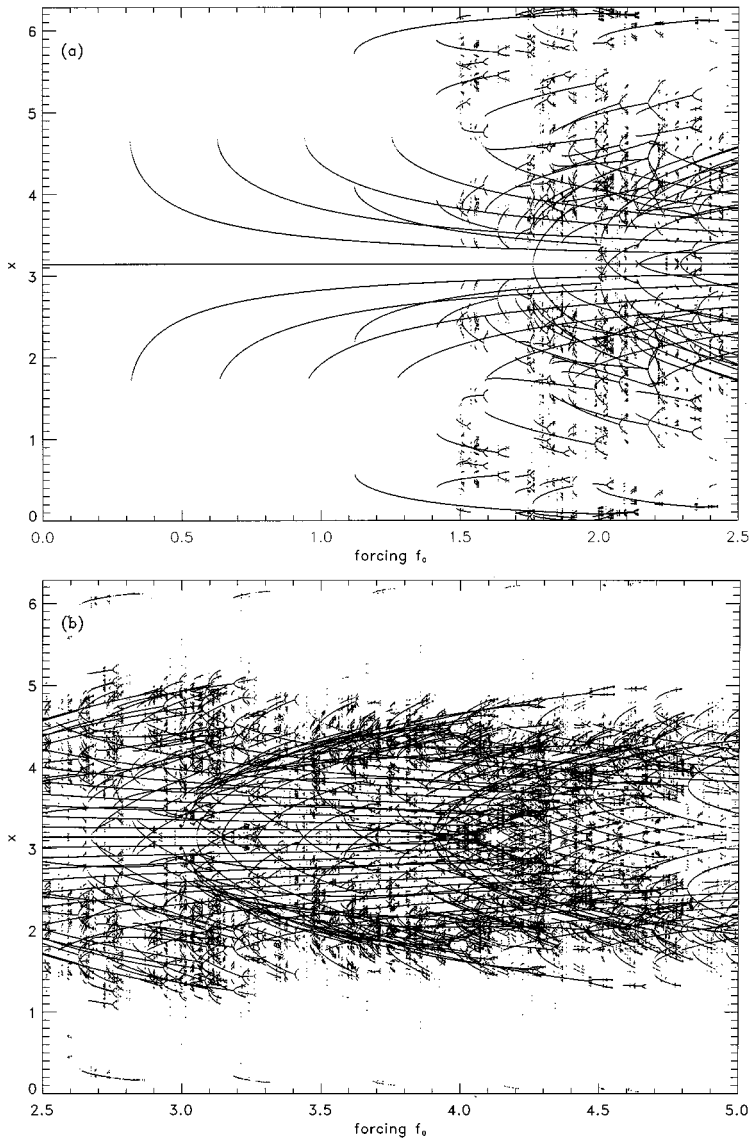

FIG. 11. Periodic attractors for fixed damping ($\nu=0.05$) depending on the forcing f_0 in the interval [0,5]: (a) phase x of the rotor, $f_0 \in [0,2.5]$; (b) phase x of the rotor, $f_0 \in [2.5,5]$.

of attractors for each family of orbits of a given period p_N. However due to the rapidly decreasing size of the basins of attraction for the high-period periodic attractors one cannot predict the highest occurring period p_N for a given forcing and damping using only numerical means.

To get an estimate on the average number of coexisting attractors of each period over the forcing interval [0,5], we count all attractors with a given period observed in this interval and divide this number by the number of f_0 values considered in this interval. This quantity can be regarded as the average number of periodic attractors of a given period per parameter value in the considered forcing interval. Plotting this average number of attractors with a period *at least* p as a function of p, we obtain a smoothing of these distributions. These distributions show a different behavior for odd and even period periodic orbits. The average number of attractors with odd period diminishes much faster than the number of even ones (Fig. 12). This reflects their different mechanisms of appearance. For the even periods, period doubling is the dominant process. Long period doubling cascades leading to relatively high periods can be observed for orbits with large basins of attraction. The attractors with odd period correspond mainly to the appearance of secondary sinks. The size of their basins of attraction decreases more rapidly with increasing period.

If we calculate the same kind of distribution for the total size of the basins of attraction of even and odd period periodic orbits, then we obtain the same scaling behavior for the basin size as a function of the period.

IV. CONCLUSIONS

We have studied a system with a very high number of coexisting attractors. Such a system can be obtained from a Hamiltonian one having a very large number of stable periodic orbits by adding a small amount of damping. Due to the dissipation the stable periodic orbits turn into sinks. Instead of the very large number a smaller number of attractors is observed for a given forcing. It seems, nevertheless, that the number of attractors can be made arbitrarily large by choosing the damping small. Families of periodic orbits of the Hamiltonian system, which yield identical points in state space, split into families of periodic attractors with different velocities. Periodic attractors belonging to the same family

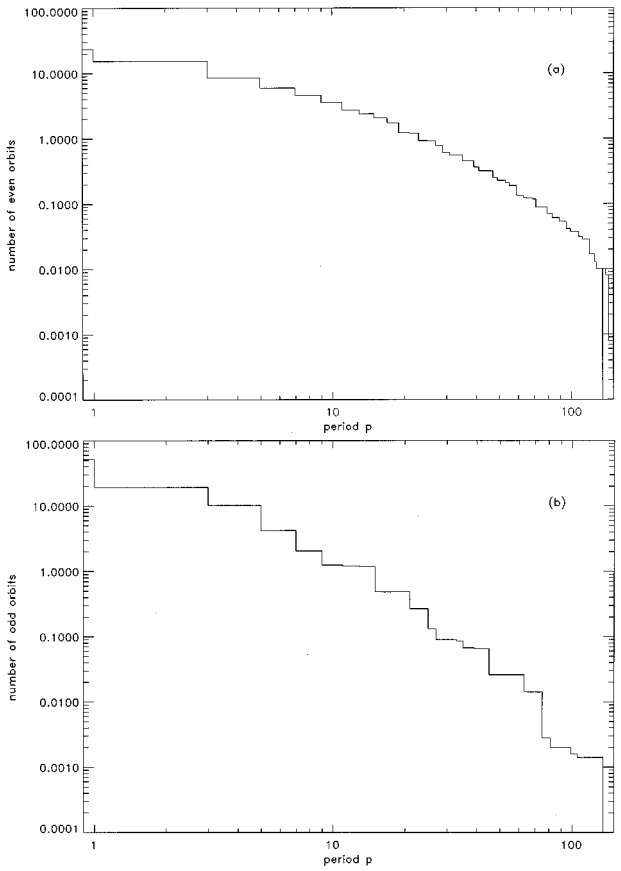

FIG. 12. Average number of periodic attractors over the whole forcing interval $f_0 \in [0,5]$ with period $\geqslant p$ vs p: (a) even period orbits; (b) odd period orbits. This average number of periodic attractors is computed as follows: We count all periodic attractors of a given period in the considered forcing interval and divide this number by the number of parameter values $f_0 \in [0,5]$ that we consider. Here we used 10^5 initial conditions for each parameter value.

of orbits exhibit the same bifurcation behavior, but their basins of attraction are of different size. Most attractors found in these systems have low periods. High period stable orbits have extremely small basins of attraction and are, therefore, difficult to detect.

In systems with many coexisting attractors as found here, the structure of their basins is very complex. They are so closely interwoven that perturbations of the magnitude of round-off error are sufficient to move an initial condition from one basin to another. This results in an extremely low predictability of the final state of the system for a given initial condition. It turns out that the dimension of the basin boundary is almost equal to the dimension of the state space.

Moreover, we have studied the double rotor which yields a four-dimensional map [24]. Here, the system's behavior is even more complex since the number of observed attractors is much higher for the same value of the damping. We find in this case more than 5000 attractors. The basins of attraction show the same complex structure as we examine the state space of initial conditions. We expect that this complexity in the bifurcation structure and the closely interwoven basins of attraction are typical properties of systems with a large number of coexisting attractors.

It is interesting to note, that for the forced damped pendulum, a system with a four-dimensional parameter space, we have not found so many attractors. The highest number of coexisting attractors that we have found was six. This result does not exclude the possibility of a high number of coexisting attractors, since we have not checked the whole four-dimensional parameter space systematically. We fixed two of the parameters and varied only the forcing and the damping. We may have, therefore, missed the regions in parameter space where a large number of coexisting periodic attractors exist.

ACKNOWLEDGMENTS

U.F. is indebted to J. Kurths, A. Pikovsky, and M. Zaks for discussions. She thanks the University of Maryland for their hospitality and acknowledges support from the DAAD. This work was also supported by DOE (Office of Scientific Computing) and NSF (Division of Physical and Mathematical Sciences). The numerical computations reported here were supported by a grant from the W. M. Keck Foundation.

[1] N. K. Gavrilov and L. P. Shilnikov, Mat. Sb. **17**, 467 (1972).
[2] S. E. Newhouse, Topology **13**, 9 (1974).
[3] P. M. Battelino, C. Grebogi, E. Ott, and J. A. Yorke, Physica D **32**, 296 (1988).
[4] L. Poon and C. Grebogi, Phys. Rev. Lett. **75**, 4023 (1995).
[5] S. E. Newhouse, Publ. Math. Inst. Hautes Etude. Sci. **50**, 101 (1979).
[6] C. Robinson, Commun. Math. Phys. **90**, 433 (1983).
[7] L. Tedeschini-Lalli and J. A. Yorke, Commun. Math. Phys. **106**, 635 (1986).
[8] H. E. Nusse and L. Tedeschini-Lalli, Commun. Math. Phys. **144**, 429 (1992).
[9] B. V. Chirikov, Phys. Rep. **52**, 265 (1979).
[10] For example: J. M. Greene, J. Math. Phys. **20**, 1183 (1979); G. Schmidt, Phys. Rev. A **22**, 2849 (1980); A. J. Lichtenberg and M. A. Lieberman, *Regular and Chaotic Dynamics* (Springer-Verlag, New York, 1992).
[11] G. M. Zaslavskii, Phys. Lett. A **69**, 145 (1978).
[12] A. J. Lichtenberg and M. A. Lieberman, *Regular and Chaotic Dynamics* (Springer-Verlag, New York, 1992).
[13] G. Schmidt and B. W. Wang, Phys. Rev. A **32**, 2994 (1985).
[14] W. Wenzel, O. Biham, and C. Jayaprakash, Phys. Rev. A **43**, 6550 (1991).
[15] A. B. Zisook, Phys. Rev. A **24**, 1640 (1981).
[16] G. R. W. Quispel, Phys. Rev. A **31**, 3924 (1985).
[17] G. Chen, G. György, and G. Schmidt, Phys. Rev. A **34**, 2568 (1986).
[18] M. A. Lieberman and K. Y. Tsang, Phys. Rev. Lett. **55**, 908 (1985).
[19] S. W. McDonald, C. Grebogi, E. Ott, and J. A. Yorke, Physica D **17**, 125 (1985).
[20] C. Grebogi, S. W. McDonald, E. Ott, and J. A. Yorke, Phys. Lett. A **99**, 415 (1983).
[21] C. Grebogi, H. E. Nusse, E. Ott, and J. A. Yorke, in *Lecture*

Notes in Mathematics, edited by J. C. Alexander (Springer-Verlag, New York, 1988), Vol. 1342, p. 220.

[22] J. W. Swift and K. Wiesenfeldt, Phys. Rev. Lett. **52**, 705 (1984).

[23] U. Feudel and W. Jansen, Int. J. Bif. Chaos **2**, 773 (1992).

[24] C. Grebogi, E. Kostelich, E. Ott, and J. A. Yorke, Physica D **25**, 347 (1987); F. Romeiras, C. Grebogi, E. Ott, and W. P. Dayawansa, Physica D **58**, 165 (1992).